Climate-driven change in the North Atlantic and Arctic Ocean can greatly reduce the circulation of the North Sea

Jason Holt[1], Jeff Polton[1], John Huthnance[1], Sarah Wakelin[1], Enda O'Dea[2], James Harle[3], Andrew Yool[3], Yuri Artioli[4], Jerry Blackford[4], John Siddorn[2], Mark Inall[5,6]

[1]National Oceanography Centre, 6 Brownlow Street, Liverpool, UK

[2]Met Office, FitzRoy Road, Exeter, UK

[3]National Oceanography Centre, Empress Dock, Southampton, UK

[4]Plymouth Marine Laboratory, Plymouth, UK

[5]Scottish Association for Marine Science, Scottish Marine Institute, Oban, UK

[6]University of Edinburgh, School of Geosciences, Edinburgh,

Corresponding author: Jason Holt (jholt@noc.ac.uk)

Key Points:

- Potential end-of-century scenarios of dramatically reduced North Sea inflow and circulation are demonstrated by downscaling experiments.
- This reduction is traced to increased shelf-slope salinity stratification and modified North Atlantic and Arctic circulation and salinity.
- The North Sea then becomes more estuarine, with some regions of substantially enhanced nutrient content and primary production.

This article has been accepted for publication and undergone full peer review but has not been through the copyediting, typesetting, pagination and proofreading process which may lead to differences between this version and the Version of Record. Please cite this article as doi: 10.1029/2018GL078878

Abstract

We demonstrate for the first time a direct oceanic link between climate-driven change in the North Atlantic and Arctic oceans and the circulation of the northwest European shelf-seas. Downscaled scenarios show a shutdown of the exchange between the Atlantic and the North Sea, and a substantial decrease in the circulation of the North Sea in the second half of the 21st Century. The northern North Sea inflow decreases from 1.2-1.3Sv ($1Sv=10^6$ m^3s^{-1}) to 0.0-0.6Sv with Atlantic water largely bypassing the North Sea. This is traced to changes in oceanic haline stratification and gyre structure, and to a newly identified circulation-salinity feedback. The scenario presented here is of a novel potential future state for the North Sea, with wide-ranging environmental management and societal impacts. Specifically, the sea would become more estuarine and susceptible to anthropogenic influence with an enhanced risk of coastal eutrophication.

Plain Language Summary

Little is known about how climate change might impact the long-term circulation of shelf-seas. In this paper, we use a high-resolution shelf-sea model to demonstrate how end-of-century changes in the wider ocean can lead to a substantial reduction in the flow of water from the North Atlantic into the North Sea. This, in turn, reduces the circulation of this sea, which becomes more influenced by rivers and less by oceanic waters. River water generally contains higher levels of nutrients and our simulations show that this future scenario leads to enhanced levels of phytoplankton growth in local regions of the North Sea. This may lead to undesirable disturbances to the marine ecosystems, such as depletion of oxygen near the seabed. The reduced circulation would also disrupt the transport of larvae around the sea and lead to increased retention of pollutants. The reduction in circulation arises from several causes relating to increased density layering at the continental shelf-edge; changes in the large-scale ocean circulation and salinity; and disruption of the density-driven circulation of the North Sea. By exploring these novel future scenarios, we emphasize the need to understand better the many ways climate change can influence the marine environment and its ecosystems.

1. Introduction

The material properties of coastal and shelf-seas (e.g. salinity, nutrients, carbon and pollutants) are largely controlled by atmospheric, oceanic and terrestrial forcing and by their circulation [*Gröger et al.*, 2013; *Holt et al.*, 2012]. However, little is known about how the circulation of shelf-seas might change under future climatic conditions. There have been many national and international programmes exploring climate impacts in the North Sea [*Quante and Colijn*, 2016], arising from the societal requirement to ensure and maintain its Good Environmental Status and its delivery of environmental services, such as fisheries and carbon sequestration [*Thomas et al.*, 2004]. To date these have largely neglected a detailed treatment of the circulation and in particular the far-field oceanic impacts on this. They have focused on the local density and wind driven circulation, and have shown only modest projected changes in circulation generally attributed to changes in wind forcing [*Schrum et al.*, 2016]. In this paper, we present downscaling shelf-sea model experiments that demonstrate the potential for a substantial reduction in the North Sea circulation arising from changes in the North Atlantic and Arctic Ocean. Similar changes in North Sea circulation were noted by *Tinker et al* [2016] in three of their eleven downscaled ensemble members with the highest climate sensitivity, but without further analysis. Here we use an analysis of regional model experiments and their driving global ocean models, along with geostrophic dynamics, to explain the nature of this potential shutdown in North Sea circulation (section

3.1). Linear models using ocean data from the Coupled Model Intercomparison Programme phase 5 (CMIP5) ensemble [*Taylor et al.*, 2012] are used to estimate the likelihood of the shutdown occurring (section 3.2). An ecosystem model is used to illustrate some potential environmental implications of such a change in the North Sea (section 3.3).

2. Methods

2.1 Model experiment design

Global coupled ocean-atmosphere climate models, as in CMIP, provide our best understanding of potential future states of the ocean. However, they currently lack the resolution and process representation to provide robust projections in shelf-seas [*Holt et al.*, 2017]. They generally do not include tides, resolve the barotropic Rossby radius on-shelf, resolve seasonal stratification or have appropriate vertical mixing schemes. These features require a downscaling approach, achieved here by running a shelf-sea model forced by boundary conditions from global climate models.

We use the AMM7 operational hydrodynamic model of the northwest European continental shelf [*O'Dea et al.*, 2012], based on the NEMO V3.2 code [*Madec*, 2008] at ~7 km resolution with 32 terrain-following vertical coordinates. Unlike other such simulations [*Adlandsvik*, 2008; *Tinker et al.*, 2016], the domain boundaries are placed sufficiently far into the ocean interior to allow ocean-shelf coupling processes to be accurately represented (Fig. 1). For atmospheric forcing we use parameters from HADGEM2 [*Jones et al.*, 2011] using the CORE parameterization [*Large and Yeager*, 2004] to calculate surface fluxes under the Representative Concentration Pathway (RCP) 8.5 (i.e. a business-as-usual climate change scenario). Wind speed and air temperature data are 6-hourly, whereas radiative and evaporation/precipitation fluxes are daily. We consider two future scenarios differing in the driving oceanic conditions. For these we use two global NEMO configurations, both forced by HADGEM2 data: ORCA1 (nominal 1^{o}, 64 levels; identified as experiment E1) and ORCA025 (nominal $1/4^{o}$, 75 levels; identified as experiment E2) [*Aksenov et al.*, 2017; *Yool et al.*, 2015; *Yool et al.*, 2013]. In both cases, surface salinity in the global model is relaxed to that of HADGEM2. We linearly transform these forcing data from the climate model 360-day year to the actual 365(6)-day year to give the correct relationship between seasonal and tidal phases. Tidal and riverine forcing, and Baltic inflow follow *O'Dea et al* [2012] and are not modified by the future climate scenario.

We initialise these AMM7 simulations from the driving global ocean model state at 1970 and run forward for 130 years to 2099 (nominal dates). We analyse the 120-year period 1980-2099, taking 30-year means over 1980-2009 to be representative of present day and 2070-2099 to be representative of end of the century conditions. The E1 AMM7 simulation is run coupled to a generic functional type ecosystem model (ERSEM [*Blackford et al.*, 2004; *Edwards et al.*, 2012]) and is used to illustrate some wider consequences of the changes in circulation. This simulates the cycling of C, N, P and Si through multiple phyto-, zooplankton, bacteria and detritus classes. Experiment E1 takes oceanic boundary conditions from the MEDUSA global ecosystem model [*Yool et al.*, 2015] run in ORCA1.

Inherent in any climate projection are multiple uncertainties, which arise from the radiative forcing scenario, the global and regional models' structure and parameters and the natural variability masking the climate change signal [*Hawkins and Sutton*, 2009]. Forced model simulations explore the system's response given specified external conditions. However, the ocean state driving the atmosphere is different from that of the driven ocean model; raising issues of scenario consistency (Fig. S3). That said, this approach is well tried

and tested in the context of global and regional forecast models, and so can provide dynamically sound, plausible future states. To some extent, this is supported by validation by observations. Comprehensive validation in numerical weather prediction model forced simulations is given by *O'Dea et al* [2012] for the hydrodynamics component and by *Edwards et al* [2012] for the ecosystem. New biases can be introduced by the climate model forcing. The hydrodynamic simulation (mean 1980-2009) remains accurate compared with WOA09 climatology [*Antonov et al.*, 2010], with the seasonal surface salinity showing spatial R^2=0.7, percentage bias (model minus observations) of 1.1% and the root mean squared error scaled by the standard deviation of the observations (RMSE/σ_{obs}) of 0.7. However, biases in the seasonal nutrient fields introduced by initialisation by the driving global model are significantly increased compared with *Edwards et al* [2012], with percentage bias increasing from 21% to 42%, and RMSE/σ_{obs} from 0.7 to 1.4. Spatial patterns are still reasonable, with R^2=0.3 compared with 0.4 for *Edwards et al* [2012].

2.2 Geostrophic dynamics

We calculate the full geostrophic transport, Q_g, by integrating the thermal wind equation downwards from the sea surface slope and a local geostrophic component, Q_{gl}, by integrating the thermal wind equation up-wards from zero velocity at the sea bed; a condition commonly used in shelf-sea observational analysis [*Hill*, 1996]. Hence, the full and local geostrophic velocities are defined as:

$$u_g = \frac{g}{f}\left[-\zeta_y - \frac{1}{\rho_0}\int_z^\zeta \rho_y dz'\right] \qquad u_{gl} = \frac{g}{f\rho_0}\int_{-h}^{z} \rho_y \, dz', \tag{1}$$

where u is the component of flow across a section, subscript y indicates an along-section derivative, g is gravitational acceleration, f is the Coriolis parameter, ρ is density, ρ_0, a reference density, z the positive upwards vertical coordinate, ζ is the sea surface height and h is the undisturbed water depth. Transports are defined as integrals in depth and along the section (length, L): $Q = \int_0^L \int_{-h}^{\zeta} u \, dzdy$. The difference between Q_g and Q_{gl} gives the remote geostrophic component, Q_{gr}. Hence, with a local wind-driven Ekman term ($Q_{ek}=\tau L/f$), for wind stress τ, and a residual, Q_{res}, the full decomposition is:

$$Q = Q_g + Q_{ek} + Q_{res} = Q_{gl} + Q_{gr} + Q_{ek} + Q_{res}. \tag{2}$$

The residual, Q_{res}, accounts for advection, bottom friction and calculation uncertainty. If we identify the component of the sea surface slope, ζ_{ly}, consistent with u_{gl} at the surface, then for zero net pressure gradient at the sea bed (with $u_{gr}=u_g-u_{gl}$):

$$\zeta_{ly} = -\frac{1}{\rho_0}\int_{-h}^{\zeta} \rho_y \, dz' \;, \zeta_y = \zeta_{ly} + \zeta_{ry}, \text{ and } u_{gr} = -\frac{g}{f}\zeta_{ry}. \tag{3}$$

Hence, the local and remote geostrophic transports can be interpreted as arising respectively from local density gradients and from non-local currents propagating as a barotropic sea-surface slope signal. The observed value of Q_{gl} can be calculated from CTD profiles along the sections. The section estimating the inflow on the western flank of the Norwegian Trench (WNT; Fig. 1) has been occupied 37 times between 1977 and 2016. We select profiles for each transect from the EN4.2 database [*Good et al.*, 2013] within 0.1° of the section and taken within 14 days. These are interpolated onto a 2m vertical grid and geostrophic currents estimated by a finite difference approach. This gives a mean observed Q_{gl} of -0.12Sv (northward), ranging from -0.47 to 0.28Sv.

3. Changes to the North Sea circulation under future climate scenarios

In the two future scenarios considered here (E1 and E2), the transport along all three pathways of Atlantic flow into the North Sea [*Sheehan et al.*, 2017; *Turrell et al.*, 1996] is substantially reduced compared with present day conditions (Figs. 1, 2). The Fair Isle Current (FIC) decreases by 48% in E1 and 35% in E2; and the East Shetland Current (ESC) decreases by 50% in E1, remaining largely unchanged in E2. The flow on the western flank of the Norwegian Trench (WNT) decreases by 173%, reversing sign in E1 during a key event over 2040-2057. In E2, WNT decreases sharply from 2040 to near zero by 2080 (by 94%). The strong poleward flowing boundary current of the North Atlantic sub-polar gyre (the Slope Current) feeds the WNT inflow. In both experiments, the slope current largely bypasses the North Sea in the end-of-century period and instead continues straight towards the Norwegian Sea. The decrease in inflow reduces the cyclonic circulation of the North Sea, notably the Dooley Current (Figs. 1, 2) by 68% in E1 and 31% in E2.

The changes in North Sea circulation are accompanied by a substantial freshening of this sea and an increase in the salinity (and density) contrast between the shelf-sea and the open ocean (Fig. 1e-f); a reduced inflow of saltier Atlantic water leads to the North Sea containing an increased fraction of riverine freshwater. We confirm the dominant role of wider oceanographic conditions in driving the circulation and density changes through an experiment that matches E1 but with present-day oceanic boundary conditions (E3; Figs. 2, 3c). This shows North Sea inflows that are reduced by a much smaller fraction than in E1: FIC by 22% rather than 48%; WNT by 54% rather than 173% and ESC by 7% rather than 50%. HADGEM2 shows a 15% decrease in wind-stress over these shelf-seas by the end of the century, which accounts for the modest decrease in inflow in E3.

These dramatic changes in the North Sea coincide with some substantial changes in the gyre circulation and salinity in the North Atlantic and Nordic Seas (Fig. 1a-c). In E1 and E2 future scenarios, the northeastward North Atlantic Current (labelled A) is fresher and positioned farther north than in present conditions. In the Nordic Seas, the East Greenland Current intensifies (B on Fig. 1a). On reaching Iceland, this current bifurcates (at C): one branch accelerates the East Iceland Current and one mixes with the Irminger Current and joins the North Atlantic current near Newfoundland. Currents are substantially stronger in E1 than in E2 [*Yool et al.*, 2015] and this is evident in the boundary conditions driving the regional model (Fig. S2). Under present day conditions, the East Iceland Current (Fig. 1d labelled D) crosses the southern Norwegian Sea and leaves the region without contact with the northwest European shelf [*Jakobsen et al.*, 2003], apart from a weak flow east of Faroe. Under the future scenarios (E1 and E2; Fig. 1e-f) the enhanced East Iceland Current flows southwest, joining the slope current, carrying water 0.5-1.0 units fresher than in present-day conditions. In E2, this is substantially intensified and also joins the slope current further north, enhancing the along-slope density gradient.

3.1 Diagnosing the circulation changes

The decrease in the western Norwegian Trench inflow (WNT) in E1 and E2, and in the East Shetland Current (ESC) inflow in E1, can be traced to the substantial increase in surface stratification at the entrance to the Norwegian Trench (Fig. 3a-c). The mean buoyancy frequency here increases by a factor of 2.0 in E1 and 1.4 in E2 and the minimum Rossby radius increases (Fig. 3d) to consistently exceed the mean radius of curvature of the entrance (~4.3 km). The Rossby radius characterises the length scale of deviations of flow from topographic steering under the Taylor-Proudman theorem [*Hide,* 1971]. Hence, as the Rossby radius increases with increasing stratification and exceeds the length scale of the

topography, this steering is relaxed and a decreasing fraction of the slope current turns the sharp corner into the Norwegian Trench (Fig. 1e labelled E). The core of the slope current moves oceanwards and the slope current largely bypasses the Norwegian Trench (Figs. 1d-f and 3a-c). In scenario E2, the strong increase in density gradient along the slope in the Faeroe-Shetland channel accelerates the slope current [*Huthnance*, 1984] (Fig. S6 and Eqn. S3). This acceleration mitigates the decrease in WNT in E2. In experiment E1, in contrast, the slope current weakly decreases.

The geostrophic decomposition for WNT (Fig. 3e-f; see Figs. S4, S5 for other sections) shows that the non-local geostrophic component (Q_{gr}), relating to the barotropic sea-surface slope, decreases markedly (from Q_{gr}=0.51Sv to -0.12Sv in E1 and from 0.50 to 0.16Sv in E2). This component scales very closely with the Rossby Radius at the entrance (R^2= 0.97 and 0.91in E1 and E2), strongly supporting the above explanation that relaxation of topographic steering leads to the reduction in WNT.

Repeat-section CTD observations across WNT show the local geostrophic current is northwards here, with Q_{gl} = -0.12Sv, somewhat larger than the modelled value of -0.07Sv in E1. In the future period, this increases to -0.26Sv (Fig. 3f) as the weaker WNT allows more freshwater from near the coast of continental Europe to flow northwards (Fig. 1 labelled F, and Figs. S6,S7), seen as a 2.0 unit salinity deficit. This further increases the density gradient across the western slope of the Norwegian Trench, enhancing the northward Q_{gl}. This positive feedback leads to a substantial increase in the now northward WNT, and the North Sea circulation has entered a new state. This new circulation state (see also [*Tinker et al.*, 2016]) can be seen as naturally arising from the usual density field, but in present conditions is inhibited by external barotropic currents (see Figs. S6,S7). In E2, Q_{gr} for WNT also closely scales with the Rossby radius at the entrance to the Norwegian Trench and Q_{gl} also increases, from -0.09 to -0.15Sv (Fig. 3f). However, the total transport (Q) remains southward, due to the acceleration of the slope current, and the runaway feedback with northwards freshwater transport is not initiated.

The decrease in the East Shetland Current (ESC) seen in E1, but not in E2, arises because the northwards freshwater transport reaches the northern North Sea (cold/salty) density maximum, which is removed in this scenario (Fig. S6). Without this density maximum the local geostrophic component of the South Shetland Current and Dooley Current is reduced (Q_{gl} decreases from 0.12 to 0.01Sv and from 0.15 to 0.08Sv respectively), and consequently the ESC substantially decreases. The reduction in ESC further reduces the salinity and another positive feedback is established. In E2 the freshwater does not reach the density maximum (Fig. S6) and the ESC remains largely unchanged. Hence, the key difference between E1 and E2 lies in whether the changes in Western Norwegian Trench inflow are sufficient to disrupt the northern North Sea density distribution and so impact the ESC.

The consistent decrease in the Fair Isle Current (FIC; Fig. 2) in both E1 and E2 can be traced upstream to the reversal in the shelf current west of Ireland (Fig. 1e-f labelled G) and in turn to ocean-shelf transport in the Celtic Sea. Drifter observations show a continuous flow pathway from the Celtic Sea to the Fair Isle channel [*Pingree et al.*, 1999]. The northward shift of the North Atlantic Current and its decreasing salinity (Fig. 1a-c) leads to a negative poleward density gradient, reducing the slope current. The resulting off-shelf geostrophic component (Fig S8 and Eqn. S2) inhibits the usual eastward wind driven on-shelf flow.

Hence, we identify two key external drivers to these changes in North Sea circulation in E1 and E2: a substantial increase in stratification in the Faeroe-Shetland Channel (for WNT and for ESC in E1) and a reduction in poleward density gradient due to freshening of the North Atlantic current (for FIC). The increase in stratification is primarily due to reduced surface salinity (65% in E1 and 75% in E2; based on Eqn S1). This cannot be accounted for by changes in surface freshwater flux (which increases by only 10%), and hence arises from lateral transport. The Faeroe-Shetland channel receives surface water from both the North Atlantic Current (eastward) and the East Icelandic Current (southward). The surface salinity of both decreases steadily. However, a lagged, detrended correlation shows the variability of WNT in E1 relates much more strongly with the surface salinity of the East Icelandic Current (max R^2=0.70, at lag 14 months) compared with that of the North Atlantic Current (maximum R^2=0.05, at lag 26 months). For E2 this is less clear: maximum R^2=0.24 at 24 months (southward) and 0.50 at 33 months (eastward). We would expect the wider oceanic changes identified here to be related to changes in Arctic sea ice and circulation, sub-polar gyre salinity and circulation, and the Atlantic meridional overturning circulation. We leave further investigation of the underlying mechanisms in the coupled ocean-atmosphere-cryosphere system to future work. However, It is worth noting that the substantial change in WNT coincides with the accelerating loss of Arctic sea ice and an ice-free East Greenland Current in the driving models [*Aksenov et al.*, 2017].

3.2 How likely is this shutdown scenario?

The CMIP5 ensemble [*Taylor et al.*, 2012] enables an estimate of the likelihood of these circulation changes occurring, through linear relations between North Sea inflows and boundary condition properties, identified above as key drivers of these changes (available for WNT and FIC; Supplement 3). Applying these linear relationships to 22 CMIP5 simulations, 20 and 18 ensemble members show a decrease in FIC and WNT inflows respectively. Compared with this distribution, the decreases in E2 are -0.37σ and -1.0σ from the median CMIP5 change for FIC (-0.09Sv) and WNT (-0.18Sv). There is less similarity between CMIP5 and E1, which gives decreases of -1.0σ and -2.7σ. Applying these relations to HADGEM2, used for atmospheric forcing, shows a similar decreases to E2 for WNT (-0.57Sv = -1.4σ), but no significant change for FIC. This arises because HADGEM2 and NEMO have different dynamics and mixing characteristics, leading to different deep-water mass properties (Fig. S3). Given the inherent uncertainty of the density and circulation in climate models at high latitudes, this analysis is itself uncertain, but provides useful guidance that these processes need to be considered among the significant marine climate impacts in this region.

We evaluate whether a reduction in oceanic inflow might be a potential impact of climate change in other regions globally using the high-resolution global model (E2), which itself shows a ~60% reduction in North Sea inflow. However, we find no evidence of a comparable reduction in inflow, in other shelf-seas around the world. This suggests that the combination of oceanic change and the particular North Sea geometry makes such an inflow reduction unique to this region. That said, increasing ocean stratification is a robust outcome of future climate projections [*Capotondi et al.*, 2012], suggesting that decoupling of currents from topographic steering arising from geostrophic theory [*Hide*, 1971] could become more widespread, though perhaps at a smaller scale than seen here in the North Sea.

3.3 Implications for the North Sea

With reduced inflow, a shelf-sea becomes less influenced by oceanic and more by riverine inputs, which are constant in these experiments. Considering dissolved inorganic

nitrogen (DIN), we turn to results from the biogeochemical model run with E1, Fig. 4. The western side of the North Sea shows a decrease in winter DIN reflecting reduced oceanic values being advected on-shelf; a consequence of the established open-ocean reduction in nutrients due to increased stratification [*Bopp et al.*, 2013; *Gröger et al.*, 2013; *Holt et al.*, 2012]. In contrast, the southern and eastern regions show a marked increase as they 'fill-up' with riverine water of higher DIN concentration. Based on a well-mixed, steady-state estimate [*Holt et al.*, 2012] the riverine contribution to DIN across the whole North Sea increases from ~8% to ~30%. These changes in winter DIN are matched by a corresponding change in annual net primary production (Fig. 4), suggesting an enhanced risk of coastal eutrophication and summer near-bed oxygen depletion events in stratified regions [*Ciavatta et al.*, 2016; *Queste et al.*, 2013]. However, increases in the southern North Sea are partly mitigated by light limitation and decreases in the north and west are augmented by local increases in summer stratification [*Holt et al.*, 2016]. Wider ecosystem impacts might also be expected. Certain commercially and ecologically important species have life cycles coupled to the North Sea circulation; e.g. Herring larvae rely on the cyclonic circulation for transport from spawning to nursery grounds [*Corten*, 2013] and deep-water coral *Lophelia pertusa* larvae are advected between oil/gas platforms, which they colonise [*Henry et al.*, 2018]. Moreover, the consequent increase in flushing time in these scenarios implies anthropogenic pollutants would be retained for longer, enhancing local impact and the risk of bioaccumulation.

4. Conclusion

Here we demonstrate how large-scale changes in ocean circulation and hydrography can have marked impacts on shelf-sea currents through a combination of stratification, geostrophic and feedback processes that are not currently captured by global climate models, nor have they been the focus of local climate impact studies. Circulation changes, such as the shutdown event identified here, would have wide-ranging impacts on shelf-sea ecosystems and the resources and services that rely on these. It is crucial, therefore, that climate change impacts of larger-scale oceanographic drivers are considered alongside the more widely investigated impacts of warming, sea level rise and ocean acidification.

Acknowledgments

This work was supported by NOC and PML's National Capability programme in Ocean Modelling. It was also supported by the UK Natural Environmental Research Council research grants: FASTNEt (NE/I030259/1), ROAM (NE/H01733X/1) and RECICLE (NE/M003477/1), and by the EU FP7 projects MYOCEAN and EuroBASIN. High Performance computing was provided by the UK Research Councils' facility ARCHER. Data from these simulations will be made available via the NERC JASMIN data server.

References

Adlandsvik, B. (2008), Marine downscaling of a future climate scenario for the North Sea, *Tellus Ser. A-Dyn. Meteorol. Oceanol.*, *60*(3), 451-458.

Aksenov, Y., E. E. Popova, A. Yool, A. J. G. Nurser, T. D. Williams, L. Bertino, and J. Bergh (2017), On the future navigability of Arctic sea routes: High-resolution projections of the Arctic Ocean and sea ice, *Marine Policy*, *75*(Supplement C), 300-317.

Antonov, J. I., D. Seidov, T. P. Boyer, R. A. Locarnini, A. V. Mishonov, H. E. Garcia, O. K. Baranova, M. M. Zweng, and J. D.R. (2010), World Ocean Atlas 2009, Volume 2: Salinity*Rep.*, 184pp pp, U.S. Government Printing Office, Washington, D.C.

Blackford, J. C., J. I. Allen, and F. J. Gilbert (2004), Ecosystem dynamics at six contrasting sites: a generic model study, *Journal of Marine Systems*, *52*, 191-215.

Bopp, L., et al. (2013), Multiple stressors of ocean ecosystems in the 21st century: projections with CMIP5 models, *Biogeosciences*, *10*(10), 6225-6245.

Capotondi, A., M. A. Alexander, N. A. Bond, E. N. Curchitser, and J. D. Scott (2012), Enhanced upper ocean stratification with climate change in the CMIP3 models, *J. Geophys. Res.-Oceans*, *117*, C04031.

Chelton, D. B., R. A. deSzoeke, M. G. Schlax, K. El Naggar, and N. Siwertz (1998), Geographical Variability of the First Baroclinic Rossby Radius of Deformation, *Journal of Physical Oceanography*, *28*(3), 433-460.

Ciavatta, S., S. Kay, S. Saux-Picart, M. Butenschön, and J. I. Allen (2016), Decadal reanalysis of biogeochemical indicators and fluxes in the North West European shelf-sea ecosystem, *Journal of Geophysical Research: Oceans*, *121*, 1824-1845.

Corten, A. (2013), Recruitment depressions in North Sea herring, *ICES Journal of Marine Science*, *70*(1), 1-15.

Edwards, K. P., R. Barciela, and M. Butenschon (2012), Validation of the NEMO-ERSEM operational ecosystem model for the North West European Continental Shelf, *Ocean Sci.*, *8*(6), 983-1000.

Good, S. A., M. J. Martin, and N. A. Rayner (2013), EN4: Quality controlled ocean temperature and salinity profiles and monthly objective analyses with uncertainty estimates, *Journal of Geophysical Research: Oceans*, *118*(12), 6704-6716.

Gröger, M., E. Maier-Reimer, U. Mikolajewicz, A. Moll, and D. Sein (2013), NW European shelf under climate warming: implications for open ocean and shelf exchange, primary production, and carbon absorption, *Biogeosciences*, *10*(6), 3767-3792.

Hawkins, E., and R. Sutton (2009), The potential to narrow uncertainties in regional climate predictions, *Bulliten of the American Meteorological Society*, *90*, 1095-1107.

Henry, L.-A., C. G. Mayorga-Adame, A. D. Fox, J. A. Polton, J. S. Ferris, F. McLellan, C. McCabe, T. Kutti, and J. M. Roberts (2018), Ocean sprawl facilitates dispersal and connectivity of protected species, *Scientific Reports*, *8*(1), 11346.

Hide, R. (1971), On geostrophic motion of a non-homogeneous fluid, *Journal of Fluid Mechanics*, *49(4)*, 745-751.

Hill, A. E. (1996), Spin Down and the dynamics of Dense Pool Gyres in Shallow Seas, *Journal of Marine Research*, *54*, 471-486.

Holt, J., M. Butenschon, S. L. Wakelin, Y. Artioli, and J. I. Allen (2012), Oceanic controls on the primary production of the northwest European continental shelf: model experiments under recent past conditions and a potential future scenario, *Biogeosciences*, *9*(1), 97-117.

Holt, J., et al. (2016), Potential impacts of climate change on the primary production of regional seas: a comparative analysis of five European seas *Progress in Oceanography*, *140*, 91-115.

Holt, J., et al. (2017), Prospects for improving the representation of coastal and shelf seas in global ocean models, *Geosci. Model Dev.*, *10*(1), 499-523.

Huthnance, J. M. (1984), Slope Currents and Jebar, *Journal of Physical Oceanography*, *14*(4), 795-810.

Jakobsen, P. K., M. H. Ribergaard, D. Quadfasel, T. Schmith, and C. W. Hughes (2003), Near-surface circulation in the northern North Atlantic as inferred from Lagrangian drifters: Variability from the mesoscale to interannual, *J. Geophys. Res.-Oceans*, *108*(C8).

Jones, C. D., et al. (2011), The HadGEM2-ES implementation of CMIP5 centennial simulations, *Geosci. Model Dev.*, *4*(3), 543-570.

Large, W. G., and S. Yeager (2004), Diurnal to decadal global forcing for ocean and sea-ice models: the data sets and flux climatologies. NCAR Technical Note NCAR/TN-460+STR, doi:10.5065/D6KK98Q6.*Rep.*

Madec, G. (2008), *NEMO reference manual, ocean dynamic component: NEMO-OPA. Note du Pole de modelisation, Institut Pierre Simon Laplace, Technical Report 27, ISSN No, 1288-1619*.

O'Dea, E. J., et al. (2012), An operational ocean forecast system incorporating NEMO and SST data assimilation for the tidally driven European North-West shelf, *Journal of Operational Oceanography*, *5*(1), 3-17.

Pingree, R. D., B. Sinha, and C. R. Griffiths (1999), Seasonality of the european slope current (Goban Spur) and ocean margin exchange, *Continental Shelf Research*, *19*, 929-975.

Quante, M., and F. Colijn (2016), *North Sea Region Climate Change Assessment*, 429 pp., Springer.

Queste, B. Y., L. Fernand, T. D. KJickells, and K. J. Heywood (2013), Spatial extent and historical context of North Sea oxygen depletion in August 2010, *Biogeochemistry*, *113*, 53-68.

Schrum, C., J. Lowe, H. E. M. Meier, I. Grabemann, J. Holt, M. Mathis, T. Pohlmann, M. D. Skogen, A. Sterl, and S. Wakelin (2016), Projected Change—North Sea, in *North Sea Region Climate Change Assessment*, edited by M. Quante and F. Colijn, pp. 175-217, Springer International Publishing, Cham.

Sheehan, P. M. F., B. Berx, A. Gallego, R. A. Hall, K. J. Heywood, and S. L. Hughes (2017), Thermohaline forcing and interannual variability of northwestern inflows into the northern North Sea, *Continental Shelf Research*, *138*, 120-131.

Taylor, K. E., R. J. Stouffer, and G. A. Meehl (2012), An Overview of CMIP5 and the Experiment Design, *Bulletin of the American meteorological society (BAMS) 93*, 485–498. .

Thomas, H., Y. Bozec, K. Elkalay, and H. J. W. de Baar (2004), Enhanced Open Ocean Storage of CO2 from Shelf Sea Pumping, *Science 304*, 1005-1008.

Tinker, J., J. Lowe, A. Pardaens, J. Holt, and R. Barciela (2016), Uncertainty in climate projections for the 21st century northwest European shelf seas, *Progress in Oceanography*, *148*, 56-73.

Turrell, W. R., G. Slesser, R. Payne, R. D. Adams, and P. A. Gillibrand (1996), Hydrography of the East Shetland Basin in relation to decadal North Sea variability, *ICES Journal of Marine Science*, *53*(6), 899-916.

Yool, A., E. E. Popova, and A. C. Coward (2015), Future change in ocean productivity: Is the Arctic the new Atlantic?, *Journal of Geophysical Research: Oceans*, *120*(12), 7771-7790.

Yool, A., E. E. Popova, A. C. Coward, D. Bernie, and T. R. Anderson (2013), Climate change and ocean acidification impacts on lower trophic levels and the export of organic carbon to the deep ocean, *Biogeosciences*, *10*(9), 5831-5854.

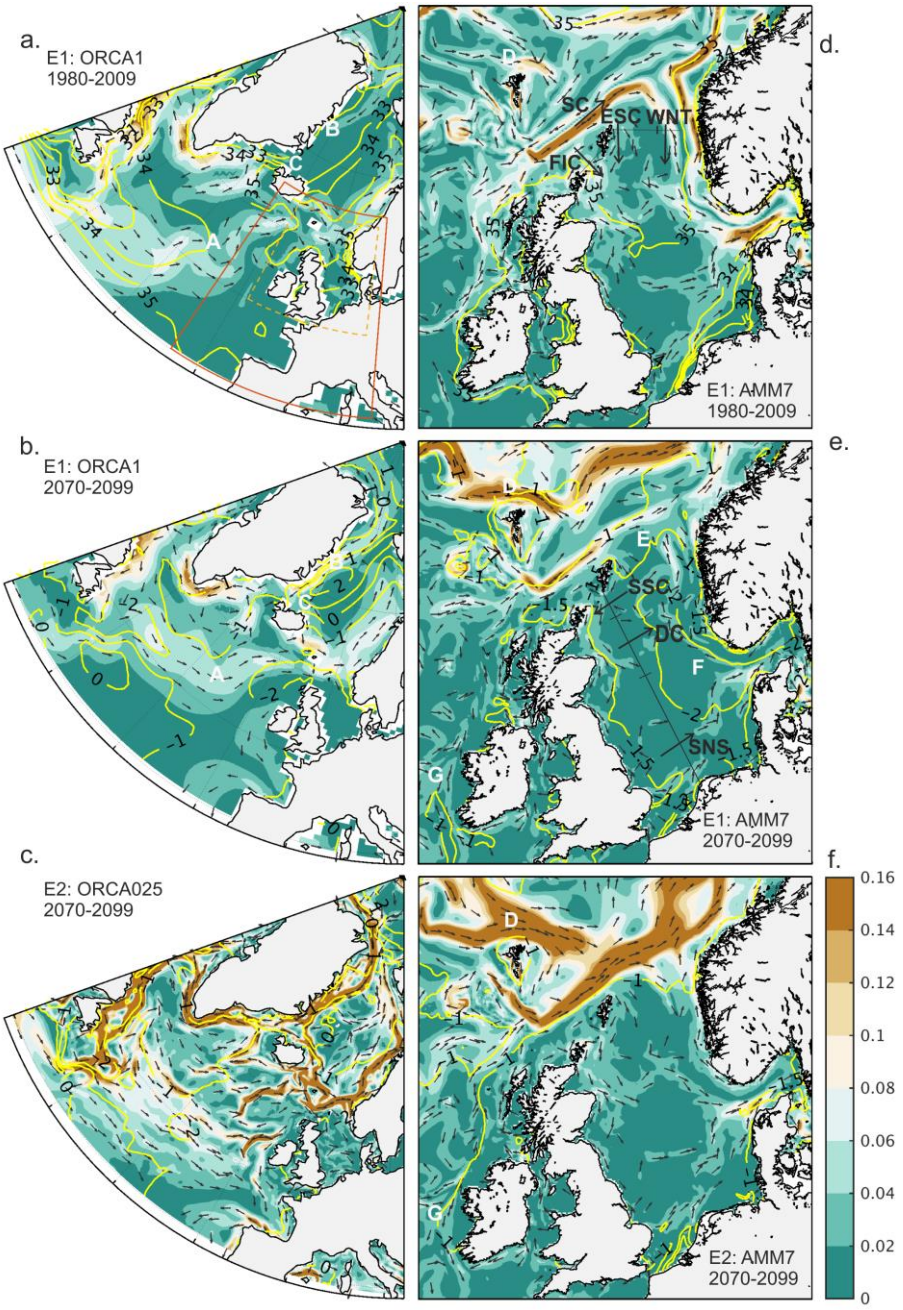

Figure 1. Depth mean currents (0 to 200m) from the two driving global NEMO models (a-c) and downscaled results (d-f) for a sub-region (dashed box on a.) of the regional model (solid on a., and Fig. S1). Colours show speed (ms^{-1}) and arrows show direction. Top figures show mean present-day conditions, centre (E1) and bottom (E2) show mean end-of-century conditions. Yellow contours in (a,d) show surface salinity, and in (b,c,e,f) show the salinity differences between future and present. (d-e) also show the sections used for time-series and geostrophic analysis (Figs. 2, 3), with arrows indicating the direction of positive transport.

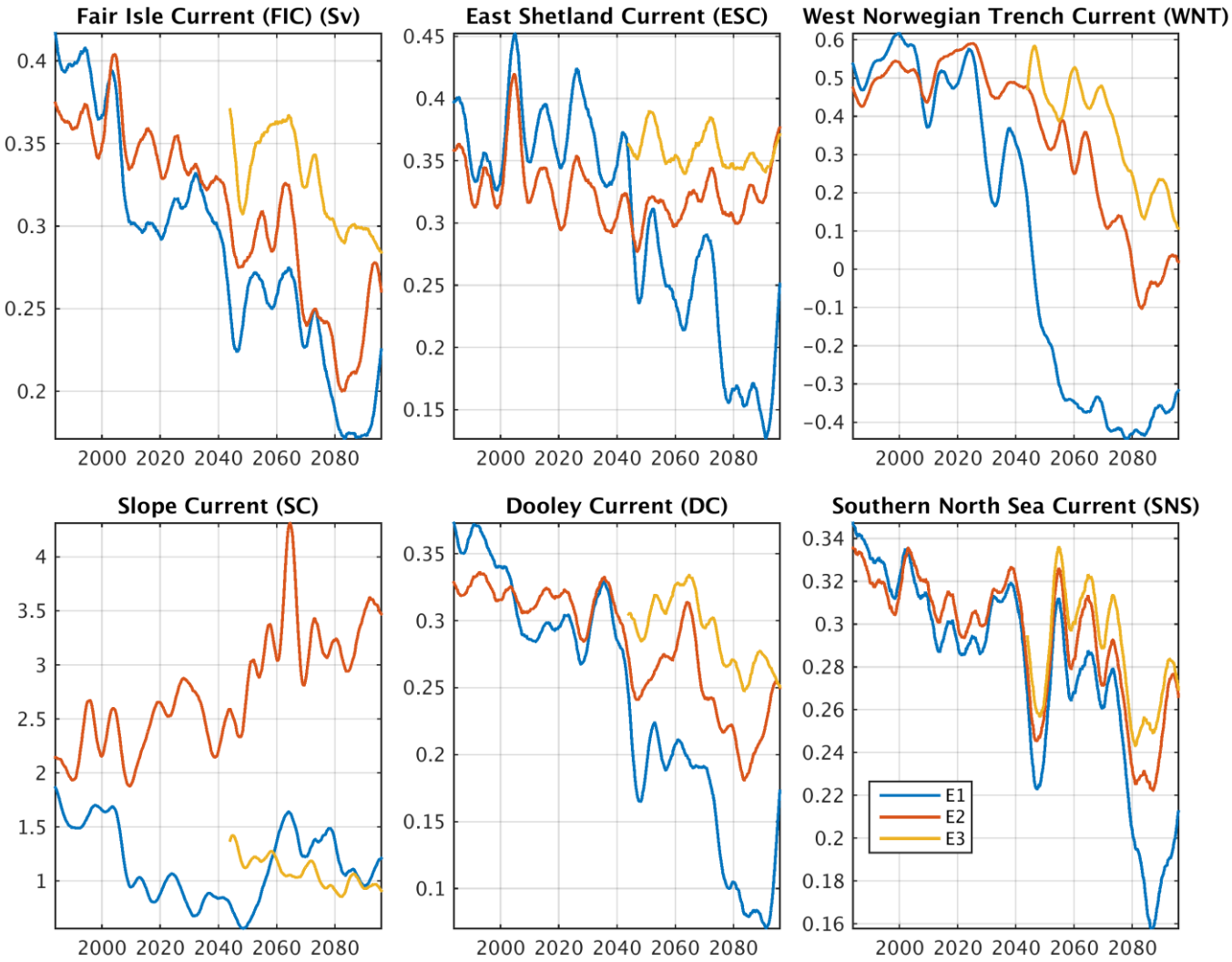

Figure 2 Time-series of volume transport (Sv) for six sections on Fig. 1. Monthly data is Gaussian filtered, σ= 2 years. Experiment E3 is restarted from E1 at 2040 with ocean boundary conditions taken from 1980-2009.

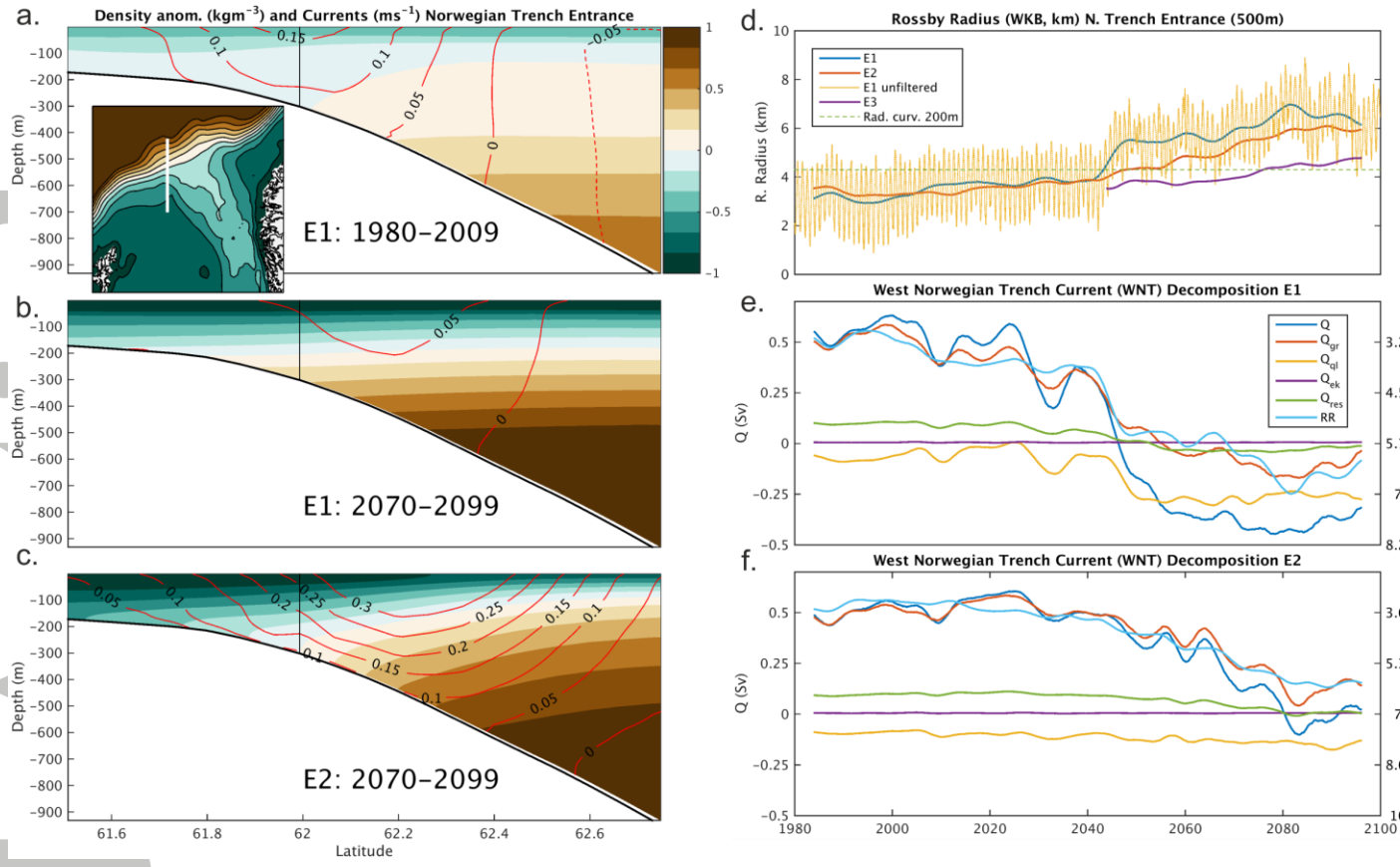

Figure 3. Latitude-Depth cross-sections of density anomaly (colours) and velocity (contours) at the entrance to the Norwegian Trench in E1: Present (a) and Future (b), and E2: Future (c). The vertical line indicates the depth of the deepest isobath that turns the corner to enter the Norwegian Trench. The insert shows isobaths at this entrance and the location of this section. The inflow is diagnosed using time-series (d) of Rossby radius (1st baroclinic, estimated from WKB approximation [*Chelton et al.*, 1998]) at the 500m isobath for E1, E2 and E3 and the geostrophic decomposition (Eqn 2) for E1 (e) and E2 (f), filtered as in Fig. 2.

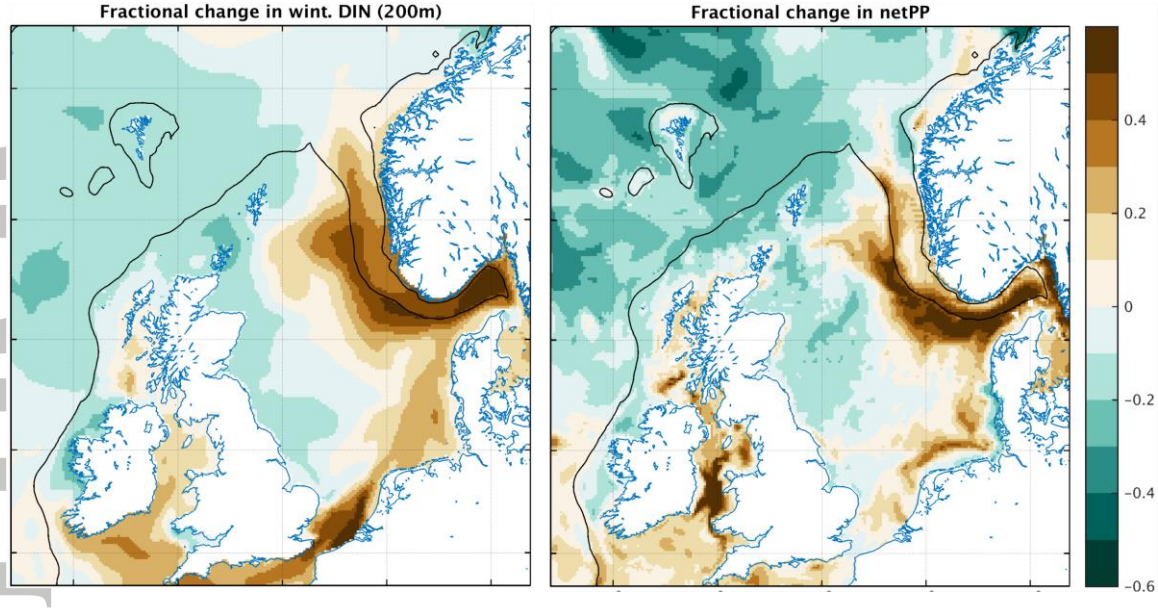

Figure 4 Fractional change (Future/Present-1) of winter Dissolved Inorganic Nitrogen (DIN) and annual net Primary Production (netPP) from the ERSEM ecosystem model in E1.